Phonon Frequencies and Widths in Dilute Cu-Au Alloys

K. M. Kesharwani and Bal K. Agrawal

Department of Physics, University of Allahabad, Allahabad, India

(Received 1 June 1972)

A detailed study of the effects of force-constant changes on phonon frequencies and widths has been made in dilute copper-gold alloys. In the calculation, a defect perturbation model which includes the change in mass at the impurity site and the changes in the nearest-neighbor central and noncentral force constants around the impurity, has been considered. Numerical calculations have been performed for the three experimentally studied Cu-Au alloys (1, 3, and 9-at.% Au). The calculated frequency shifts and the phonon widths compare well with the results of recently performed inelastic-neutron-scattering experiments on dilute alloys, i.e., copper containing 1- and 3-at.% Au as impurities. In Cu–9.0-at.% Au where interference effects of two or more than two impurities are expected, the resonant frequency calculated in low-concentration theory is found to be smaller than the experimentally measured frequency by about 15%. The effects of the lattice expansion caused by the impurity atoms on the phonon frequencies has been accounted for in a manner which does not involve any arbitrary parameter. The observed discrepancies in the high-frequency region suggest the need of a theory for the lattice expansion effect which properly takes into account the changes in the electron screening in alloys.

I. INTRODUCTION

A number of inelastic-coherent-neutron-scattering experiments[1-6] have been performed to study the effects of a low concentration of impurities on the phonons of a crystal. In these studies, two defect systems, i.e., Cr-W alloys and Cu-Au alloys, have been widely investigated. The low-concentration theory of Elliott and Maradudin[7] has been found to be inadequate to explain the observed phonon shifts and widths. The observed discrepancies between theory and experiment may arise either due to interference effects between the clusters of the impurities or due to a neglect of changes in the interatomic forces around the impurity atoms, or both. A number of calculations have been performed in the coherent-potential approximation for a high concentration of isotopic impurities[8] or δ-function perturbations.[9] However, the possibility of a complete understanding of these discrepancies on the basis of a high-concentration theory has been ruled out by a number of experimental investigations[3,6] performed on very dilute alloys. Thus the necessity for the development of a theory which also includes the changes in the host-impurity interactions was envisaged.

In an earlier paper[10] (hereafter referred to as I), the present authors have made a detailed study of the effects of force-constant changes on the frequencies and the widths of phonons in a chromium crystal due to a low concentration of tungsten atoms. An over-all good agreement with the experiment was observed there except in some frequency regions. It was shown that the effects due to the change in the lattice parameter on alloying should also be considered to understand these experiments.

The other dilute alloys which have been widely studied are the Cu-Au alloys. The additional advantage with this system is that we have more experimental information[11] about the mode-Grüneisen parameters (defined in the text), i.e., the experimental values of elastic-constant Grüneisen parameters are available while the same are unknown in a chromium crystal. These Grüneisen parameters for zero wave vector may be utilized to determine the wave-vector dependence of the Grüneisen parameters away from zero wave vector, the latter being required to discuss the lattice expansion effect.

The first measurements of phonon shifts and widths in Cu–9.3-at.% Au were carried out by Svensson *et al.*[1] along the $(0, 0, \xi)$ symmetry direction for the transverse branch. Later on, Svensson and Brockhouse[2] performed experiments on Cu–3.0-at.% Au for the $(0, \xi, \xi)T_1$ branch [polarization vectors parallel to $(0, \bar{\xi}, \xi)$]. Recently, more detailed studies have been made by Svensson and Kamitkahara[3] in Cu-Au alloys containing 1-, 3-, and 9-at.% gold atoms in the $(0, 0, \xi)T$, $(0, \xi, \xi)T_1$, and $(0, 0, \xi)L$ polarization branches.

In the present paper, we have investigated the inelastic-neutron-scattering experiments performed by Svensson and Kamitkahara[3] on Cu alloys containing 1-, 3-, and 9-at.% gold atoms. A defect-perturbation model including the changes in the mass and nearest-neighbor central and noncentral force constants has been used. The known elastic-constant Grüneisen parameters have been employed to determine the effect of lattice expansion on the phonon frequencies. Recently Brüno and Taylor[12] have also calculated the phonon shifts and widths in Cu–3.0-at.% Au. We have compared their results with those of the present ones in Sec. V.

A very brief account of the low-concentration theory is given in Sec. II. The lattice dynamics for the pure copper and the calculations of Green's functions are discussed in Sec. III A. The shifts in phonon frequencies and widths due to force-constant changes are calculated in Sec. III B. The lattice-expansion effect due to the presence of gold impurities on the phonon frequencies is discussed in Sec. III C. The calculated shifts and widths for each alloy are compared with the inelastic-coherent-neutron-scattering results in Sec. IV. A comparison with Brüno and Taylor's[12] results for Cu-3.0 at.% Au is made in Sec. V. The observed discrepancies between theory and experiment are discussed in Sec. VI where the necessity of a theory accounting for the lattice-expansion effects in a proper manner is emphasized.

II. THEORY

For the details of the one-phonon neutron-scattering cross section and the configurationally averaged phonon propagator in the low-concentration limit, we refer to an earlier paper.[10]

For certain symmetry directions, i.e., for wave vectors lying along $(0, 0, \xi)$, $(0, \xi, \xi)$, and (ξ, ξ, ξ) directions $(\xi = k/k_{max})$ in cubic crystals, there is no mixing of phonon-polarization branches labeled below by s. The shifts $\Delta\omega$ in phonon frequencies in these directions are approximately given by

$$\omega - \omega_{\vec{k},s} = \Delta\omega = \frac{\mathrm{Re}\underline{\Sigma}(\vec{k}, s)}{\omega + \omega_{\vec{k},s}}$$

$$\simeq \frac{\mathrm{Re}\underline{\Sigma}(\vec{k}, s)}{2\omega_{\vec{k},s}}, \qquad (1)$$

in the first approximation.

The phonon full widths S (at half-maximum) are determined by

$$S = \frac{2\,\mathrm{Im}\underline{\Sigma}(\vec{k}, s)}{\omega + \omega_{\vec{k},s}}$$

$$\simeq \frac{\mathrm{Im}\underline{\Sigma}(\vec{k}, s)}{\omega_{\vec{k},s}}, \qquad (2)$$

in the first approximation.

Here $\omega_{\vec{k},s}$ and ω are the phonon frequencies in the perfect and the imperfect crystals, respectively. $\underline{\Sigma}(\vec{k}, s)$ is the self-energy of phonons for the perfect crystal eigenstate $|\vec{k}, s\rangle$ and is given by

$$\underline{\Sigma}(\vec{k}, s) = \langle\vec{k}, s\,|\,\underline{\Sigma}\,|\,\vec{k}, s\rangle. \qquad (3)$$

The first-order self-energy [see Eq. (21) of I] in the Elliott–Taylor approximation can be expressed as[13]

$$\underline{\Sigma}_1 = c\underline{t}\,[\underline{I} - c\underline{g}(z)\underline{t}]^{-1}$$

$$= c\underline{p}(\omega^2)[\underline{I} + (1 - c)\underline{g}(z)\underline{p}(\omega^2)]^{-1}, \qquad (4)$$

where the t matrix for a single impurity is defined by

$$\underline{t}(z) = \underline{p}(\omega^2)[\,\underline{I} + \underline{g}(z)\underline{p}(\omega^2)]^{-1}. \qquad (5)$$

Here z is the squared complex frequency $\omega^2 + 2i\omega\eta$ in the limit $\eta \to 0^+$; c is the fractional concentration of impurities. $\underline{g}(z)$ is the Green's-function matrix for the perfect lattice lying in the impurity space of a single defect and is defined by

$$\underline{g}(z) = (\underline{L}_0 - z\underline{I})^{-1}, \qquad (6)$$

where $\underline{I}$ is the unit matrix and $\underline{L}_0$ is the mass-reduced dynamical matrix for the perfect lattice. The perturbation matrix $\underline{p}(\omega^2)$ is the perturbed part in the dynamical matrix for a crystal containing a single defect which can be written as

$$\underline{L} = \underline{L}_0 + \underline{p}(\omega^2). \qquad (7)$$

For the lowest order in impurity concentration, the self-energy turns out to be

$$\underline{\Sigma}_1 = c\underline{t}. \qquad (8)$$

In order to make the calculation of the t matrix tractable, one exploits the symmetry of the perturbation of the defect. This reduces the problem of calculating the t matrix in various pertinent irreducible representations. Again, for details we refer to an earlier paper.[14]

III. CALCULATIONS AND RESULTS

The metal copper and its alloys with gold crystallize in fcc structures. If we assume a perturbation around an impurity in which we consider a change in mass at the defect site and the changes in the first-neighbor central and the noncentral force constants of de Launay type, the matrix $\underline{p}(\omega^2)$ is of dimension 39×39. The point-group symmetry is O_h and the irreducible representations F_{1u}, F_{2u}, F_{1g}, F_{2g}, E_g, E_u, A_{2u}, A_{1g}, and A_{2g} are seen to occur. The t matrix in these irreducible representations for a diatomic fcc lattice has been obtained earlier by one of the authors.[14] For a monatomic fcc lattice, the pertinent expressions can readily be obtained.

A. Lattice Dynamics and Green's Functions

Copper is a transition metal with one atom per unit cell. A six-neighbor force-constant model has been used by Svensson et al.[16] to understand the dispersion curves measured by neutron-scattering experiments. The electron-gas contribution is not considered in this type of calculation. In the present calculation we have employed Kreb's model[15] for the determination of eigenfrequencies and the eigenvectors in copper. In this model, one takes into account the first- and second-neighbor ion-ion interactions of central type and also the effect of electrons on the motions of ions via the screened
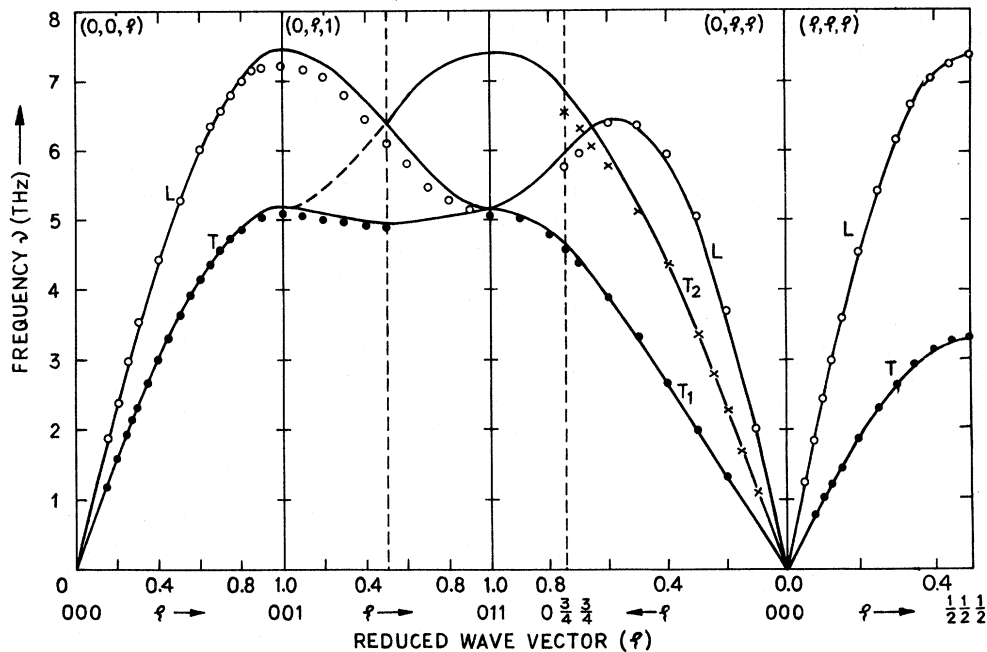
FIG. 1. Dispersion curves for copper. O, ●, and × denote the experimental data of Svensson *et al.* (Ref. 16) for the longitudinal and the first and second transverse branches, respectively.

Coulombic interaction. The employed values of the elastic constants at room temperature (300 °K) are $C_{11} = 16.839 \times 10^{11}$ dyn cm^{-2}, $C_{12} = 12.142 \times 10^{11}$ dyn cm^{-2}, and $C_{44} = 7.539 \times 10^{11}$ dyn cm^{-2}. The lattice parameter a used is 3.6147 Å. The values of the two parameters which appear in the calculation of the electron contribution to the dynamical matrix (i.e., effective change Z and Bohm–Pines parameter β) are taken as 1 and 0.353, respectively. While performing calculations, we have also considered the wave-vector dependence of the screening parameter k_c given by Eq. (34) of I.

The dynamical matrix for a face-centered-cubic lattice was diagonalized to obtain the eigenfrequencies and polarization vectors. The calculated pho-

non frequencies have been compared with the results of inelastic-neutron-scattering experiments obtained by Svensson *et al.* [16] in the symmetry directions $(0, 0, \xi)$, $(0, \xi, \xi)$, (ξ, ξ, ξ), etc. in Fig. 1. Very good agreement with the experiment is observed. After making several trials, it was found that the use of 8000 points in the first Brillouin zone gives reasonably good values for the phonon density of states. This phonon density of states has been plotted in Fig. 2.

The various Green's functions were calculated by a method described in I. In order to perform the integration, the whole frequency range was divided into 60 bins and the histograms were obtained at the center of each bin. A value of 0.33 in units of
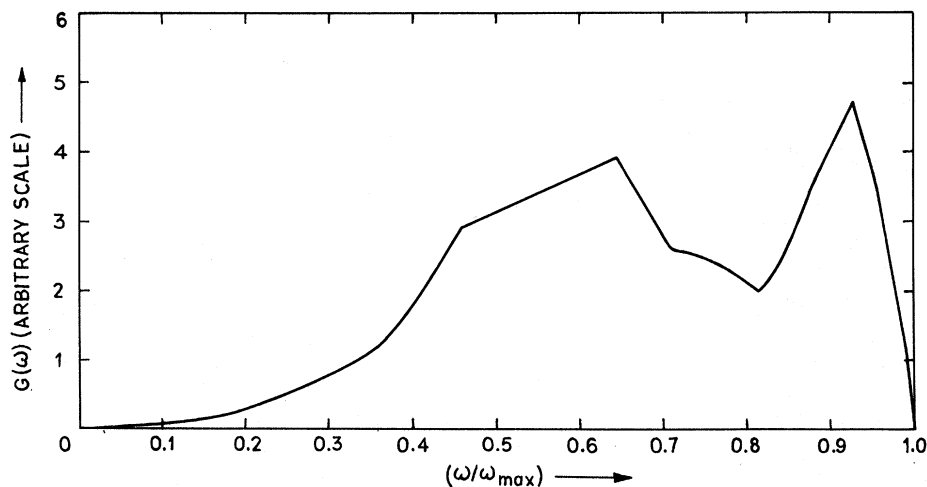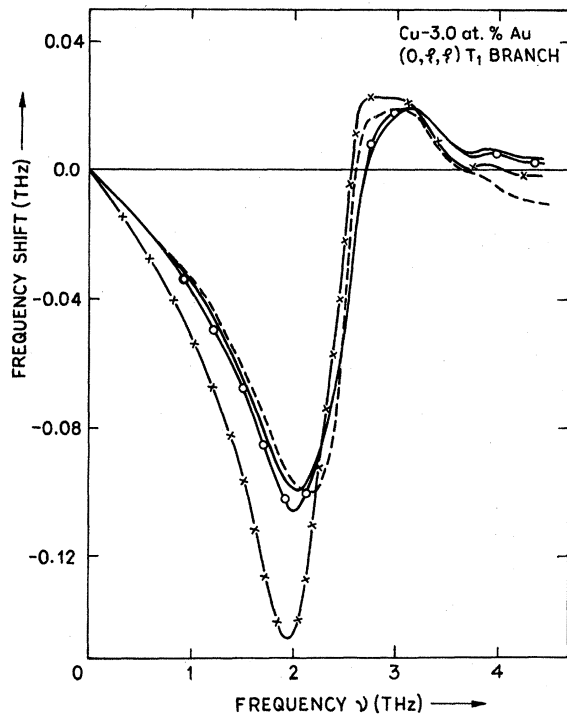

FIG. 2. Density of states for copper.

FIG. 3. Cu–3.0-at.%-Au alloy: frequency shifts for $(0, \xi, \xi)$ T_1 branch (no volume effect); (– – – –) mass defects only; (——) $\lambda = 0.8 \times 10^{26}$ sec^{-2} and $\lambda' = -0.1 \times 10^{26}$ sec^{-2}; (–×–) $\lambda = 0.8 \times 10^{26}$ sec^{-2} and $\lambda' = -0.2 \times 10^{26}$ sec^{-2}; (–O–) $\lambda = 0.7 \times 10^{26}$ sec^{-2} and $\lambda' = -0.1 \times 10^{26}$ sec^{-2}.

bin width for the increment in the frequency was used in the integrations. This finite increment in the frequency minimized the spurious fluctuations appearing in the calculation of Green's functions.

B. Effects of Force-Constant Changes

We have studied the effects of force-constant changes on the frequencies and widths of phonons by varying the central and the noncentral parts (λ and λ') independently. The calculations for the three impurity concentrations, i.e., 1-, 3-, and 9-at.%-Au atoms have been performed by using Eqs. (1) and (2). As a representative case, the effects of force-constant changes on the frequency shifts seen in the case of a Cu–3-at.%-Au system are demonstrated for the $(0, \xi, \xi)T_1$ and $(0, 0, \xi)T$ branches in Figs. 3 and 4. We find that the frequency shifts in the $(0, \xi, \xi)T_1$ branch are, in general, more sensitive to force-constant changes as compared to the shifts in the $(0, 0, \xi)T$ branch. Further, analogous to Cr-W alloys reported in I, the qualitative effects of the changes in λ and λ' are similar but greatly differ in magnitude. For example, the frequency shifts in the $(0, 0, \xi)T$ branch are about four times more sensitive to λ' in comparison to λ throughout the whole frequency range. In the $(0, \xi, \xi)T_1$ branch, the shifts are seen to be

about nine times more sensitive to λ' in comparison to λ in a region prior to resonance, and four times thereafter.

Regarding phonon widths, they are less affected by force-constant changes in the $(0, 0, \xi)$ direction as compared to $(0, \xi, \xi)$ direction. The maximum phonon widths (full width at half-maximum) which appear at the resonant frequencies, increase with a decrease in λ and λ'.

As mentioned earlier, the first-order self-energy can be calculated by using either Eq. (4) or (8). The differences in the results obtained by using Eqs. (4) and (8) are not very significant except in the resonant frequency region, e.g., for a Cu–3-at.%-Au alloy the over-all differences in the results obtained by using Eq. (4) or (8) are only 1% while these differences are only 3% near the resonant frequency. The resonant frequency is seen to be shifted slightly to the higher-frequency side in the Elliott–Taylor approximation. Thus the results in the Elliott–Taylor approximation[13] are not appreciably different from those obtained in the lowest-order concentration theory.

In the calculations, one may use the values of the Green's functions determined for the pure unexpanded crystal lattice or, to be very cautious, one may use the values of Green's functions obtained for the expanded lattice, i.e., the effective lattice. In order to see the difference in the results obtained with the use of two sets of Green's functions, we have performed some calculations and found that the results are practically the same. Slight changes in the maximum negative and positive fre-
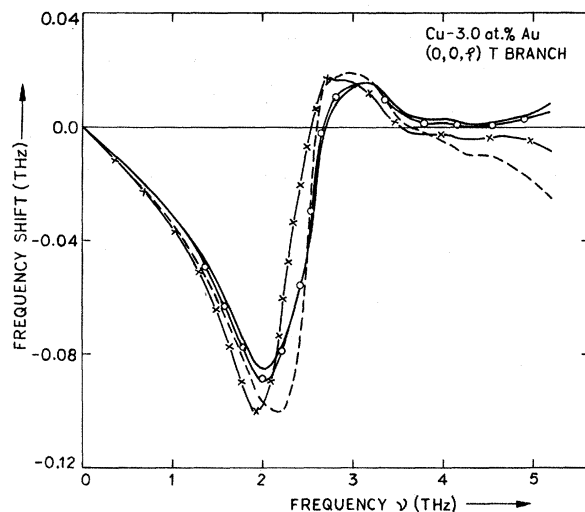

FIG. 4. Cu–3.0-at.%-Au alloy: frequency shifts for $(0, 0, \xi)$ T branch (no volume effect); (– – – –) mass defects only; (——) $\lambda = 0.8 \times 10^{26}$ sec^{-2} and $\lambda' = -0.1 \times 10^{26}$ sec^{-2}; (–×–) $\lambda = 0.8 \times 10^{26}$ sec^{-2} and $\lambda' = -0.2 \times 10^{26}$ sec^{-2}; (–O–) $\lambda = 0.7 \times 10^{26}$ sec^{-2} and $\lambda' = -0.1 \times 10^{26}$ sec^{-2}.
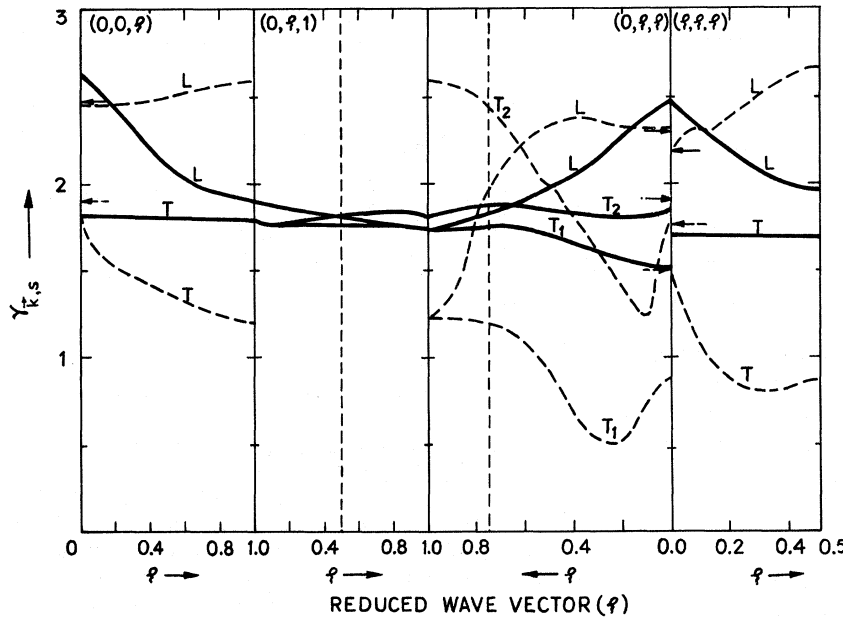
FIG. 5. Structure of Grüneisen-mode parameter $\gamma_{\vec{k},s}$ against the reduced wave vector ξ in copper. The full curve represents the results of the present calculation. The experimental elastic-constant Grüneisen parameters are shown by different types of arrows, i.e., $\rightarrow$ denotes value for the longitudinal branch; $----\rightarrow$ and $-\cdot-\cdot\rightarrow$ denote the values for the two transverse branches, respectively. The dashed curves show the results of Brüno and Taylor (Ref. 12).

quency shifts have been observed near the resonant region but these effects are not very significant. Thus, we present here the results obtained by utilizing the Green's functions for the pure-copper lattice.

C. Lattice Expansion Effect

In I, it was found that the effects on the phonon frequencies due to the expansion of the pure-chromium lattice on alloying should be taken into account. The same is found to be true in Cu-Au alloys. The lattice of the metal copper expands when it is doped with gold atoms, e.g., the volume expansion due to 1-at.%-Au atoms is 0.56%. The phonon frequencies of the effective lattice, i.e., the expanded pure lattice, are different from those of the pure one. This effect can be accounted for if one knows the values of the Grüneisen-mode parameters ($\gamma_{\vec{k},s} = -\partial \ln\omega_{\vec{k},s}/\partial\ln V$; V is the crystal volume) for the whole frequency range. The mode γ's, in general, exhibit a structure, i.e., they vary with the phonon wave vector. However, the values of the mode γ's in copper for different symmetry directions are known only for zero wave vector, i.e., for $\vec{k} = 0$.[11] Hence the immediate problem before us is to study the variations of mode γ's with phonon wave vector. We investigate it in the following manner.

Since the mode γ's for $\vec{k} = 0$ are known, we utilize them to determine the elastic constants for the effective lattice. These elastic constants are employed to calculate the phonon frequencies and the polarization vectors for the effective lattice. The calculated values of the mode γ's for different wave vectors in three symmetry directions, i.e.,

$(0, 0, \xi)$, $(0, \xi, \xi)$, and (ξ, ξ, ξ), are shown in Fig. 5. We observe that the mode γ's for the transverse branches do not show much variation with phonon wave vector and are almost constant. This result is in agreement with our assumption used earlier in the case of Cr-W alloys. But the behavior of mode γ's is different for longitudinal branches where its value decreases at high frequencies; e.g., there is a decrease of about 27.5% along $(0, 0, \xi)$ direction. This behavior is not surprising because the electron screening effect considered in Kreb's model[15] is essentially a volume-dependent effect and depends on the bulk modulus of the electron gas. The longitudinal phonons are much more affected by this electron-gas contribution in comparison to the transverse ones.

In general, the experimental elastic-constant mode γ's are reproduced in all the phonon-polarization branches except for very small discrepancies in some branches. These discrepancies are easily understandable. The reason is that usually the elastic constants obtained by inelastic-neutron-scattering data do not tally with the values obtained by velocity measurements. In a phenomenological lattice model, the latter values of the elastic constants are used as input data and fits are obtained with the inelastic-neutron-scattering data. Consequently, the input data of elastic constants are not always reproduced and some discrepancies occur.[16] For example, in the present Kreb's model, the above discrepancies between input and output data are of the order of 1, 3, and 10% for C_{11}, C_{44}, and C_{12}, respectively. In Table I, we compare the changes in the elastic constants because of the expansion of the lattice used as input data along with

TABLE I. Input and output data for the changes in the elastic constants due to expansion of the copper lattice on alloying with gold (in units of 10^{11} dyn cm^{-2}).

Changes in the elastic constants	Input data	Output data
ΔC_{11}	−1.45	−1.73
ΔC_{12}	−1.06	−1.12
ΔC_{44}	−0.52	−0.63

the corresponding values obtained in Kreb's model. In view of the above discussion, these small discrepancies between the input and output data can be understood. It may be noted that in Fig. 5 we have plotted the values of mode γ's obtained directly by the definition of the mode parameters, i.e.,

$$\gamma_{\vec{k},s} = -\frac{\partial \ln \omega_{\vec{k},s}^*}{\partial \ln V}.$$

IV. COMPARISON WITH EXPERIMENT

To begin, the dilute alloy containing 3.0-at.%-Au atoms seems to be the most appropriate host-impurity system because maximum information is available in this particular alloy. A more dilute alloy which contains 1.0-at.% Au would have been the best choice, but in this system on one hand the phonon widths could not be measured experimentally, while on the other hand the probable errors in the measured maximum frequency shifts are as large as 50 or 80% in the $(0, 0, \xi)T$ or $(0, \xi, \xi)T_1$ branch. The other well-studied system is the alloy containing a high concentration of impurities, i.e., 9-at.% Au, but the interference effects between the subspaces of two or more than two impurity atoms are inevitable (see Sec. IV C), and the low-concentration theory is not expected to be adequate for treating this alloy.

The experimentally measured frequency shifts and widths in $Cu_{0.97}Au_{0.03}$ have been fitted by varying the parameters λ and λ'. A number of sets for (λ, λ') were chosen to reproduce approximately the position of the resonant frequency, i.e., $\omega_r = 2.75$ THz observed in the measured phonon widths. These sets were then utilized to match the experimentally measured maximum frequency shifts. In this fitting procedure, attention was also given to reproducing the observed small frequency shifts in the high-frequency region. The volume-expansion effect discussed in Sec. III C has also been considered in the calculations. The values of the force constants for the pure-copper lattice and the changes due to a single gold atom are shown in Table II. The results of the best fits for the three impurity concentrations are presented in Figs. 6–19. For the sake of comparison in these figures, we also show the results of the mass-defect theory[7]
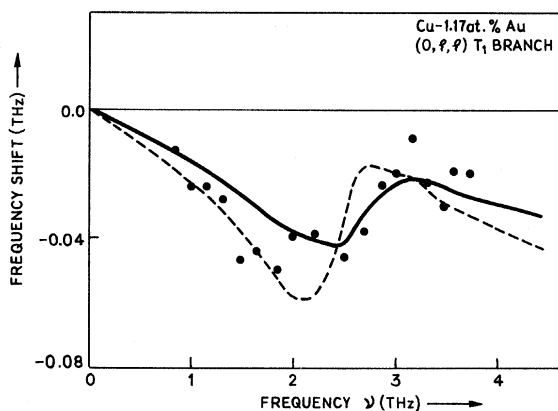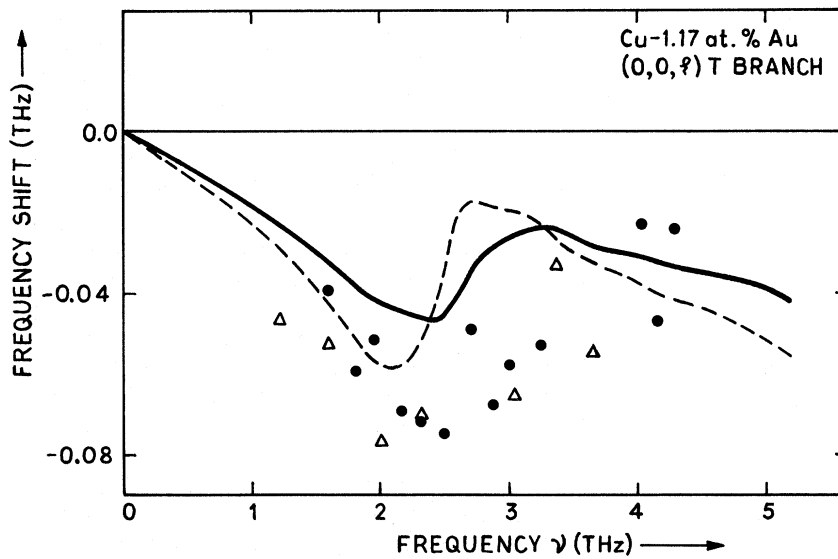

FIG. 6. Cu-1.17-at.%-Au alloy: the calculated frequency shifts in $(0, \xi, \xi)$ T_1 branch (volume effect included). The solid curve shows the calculations with force-constant changes ($\lambda = 1.200 \times 10^{26}$ sec^{-2} and λ' = −0.025 × 10^{26} sec^{-2}) and the dashed curve represents the calculations of mass defects only. Solid circles represent the measurements of Svensson and Kamitkahara (Ref. 3).

after accounting for the volume-expansion effect. We now discuss the results for each alloy separately.

A. Cu—1.0-at.% Au

The nominal gold concentration obtained by Svensson and Kamitkahara[3] was 1.17%. Consequently, the calculations have been performed for this concentration $c = 0.0117$. The calculated frequency shifts have been compared with the experimental ones in Figs. 6 and 7. Although no experimental results for phonon widths have been reported for this alloy due to their small magnitudes, for the sake of completeness, we report here the results of the calculated phonon widths in Figs. 8

TABLE II. Mass-reduced force constants for pure copper and the changes in them due to gold at room temperature (in units of 10^{26} sec^{-2}).

Force constants	Copper	Parameters	Changes due to gold atoms Present value	Brüno-Taylor values[a] (calculated)
α_1[b]	3.175	λ[c]	1.200	0.643
β_1[d]	−0.197	λ'[e]	−0.025	−0.197, 0.052
α_2[f]	−0.046			

[a]Reference 12.
[b]α_1, first-neighbor central force constant.
[c]λ, change in first-neighbor central force constant due to impurity atoms.
[d]β_1, first-neighbor noncentral force constant.
[e]λ', change in first-neighbor noncentral force constant due to impurity atoms.
[f]α_2, second-neighbor central force constant.

FIG. 7. Cu−1.17-at.%-Au alloy: the calculated frequency shifts in $(0, 0, \xi)$ T branch (volume effect included). The solid curve shows the calculations with force-constant changes $(\lambda = 1.200 \times 10^{26}$ sec^{-2} and $\lambda' = -0.025 \times 10^{26}$ sec$^{-2})$ and the dashed curve represents the calculations of mass defects only. The solid circles and the triangles represent the measurements of Svensson and Kamitkahara (Ref. 3).

and 9. In the $(0, \xi, \xi)T_1$ branch, the calculated shifts compare very well with the experimental ones.

In the $(0, 0, \xi)T$ branch, the calculated negative shifts are, on the whole, smaller than the experimental ones, but the shape of the curve has been well reproduced. However, the experimentally measured shifts are quite uncertain because of the possibility of relatively large systematic errors in the experiment. For example, these errors may be as large as 50% (or 80%) of the maximum observed shifts in the $(0, 0, \xi)T$ or $[0, \xi, \xi)T_1]$ branch.

B. Cu−3.0-at.% Au

For this alloy, the calculated values for the phonon shifts and widths have been shown in Figs. 10–13 along with experimental measurements. For the $(0, \xi, \xi)T_1$ branch, in the low-frequency region, the calculated shifts compare well with the experimental ones, whereas in the high-frequency region the calculated values are larger. The situation is different for the $(0, 0, \xi)T$ branch, where an overall reasonable agreement is observed throughout the whole frequency range. Any attempt to remove the discrepancy in the high-frequency region observed in $(0, \xi, \xi)T_1$ branch by varying λ and λ' was
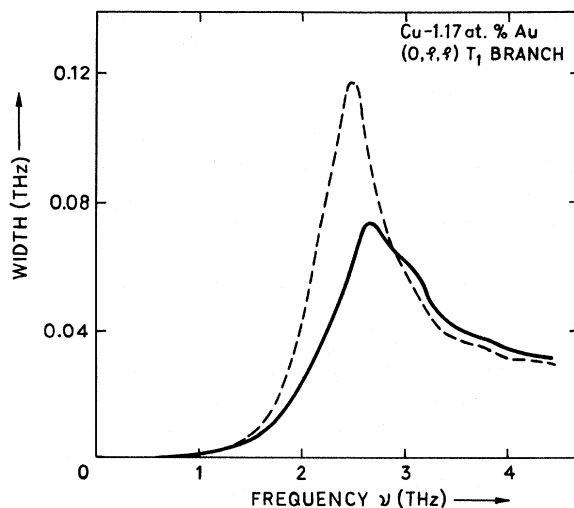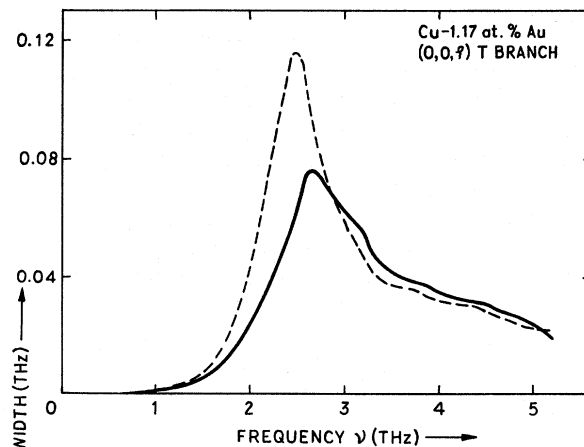

FIG. 8. Cu−1.17-at.%-Au alloy: the calculated phonon widths in $(0, \xi, \xi)$ T_1 branch. The solid curve shows the calculations with force-constant changes $(\lambda = 1.200 \times 10^{26}$ sec^{-2} and $\lambda' = -0.025 \times 10^{26}$ sec$^{-2})$ and the dashed curve represents the calculations of mass defects only.

FIG. 9. Cu−1.17-at.%-Au alloy: the calculated phonon widths in $(0, 0, \xi)$ T branch. The solid curve shows the calculations with force-constant changes $(\lambda = 1.200 \times 10^{26}$ sec^{-2} and $\lambda' = -0.025 \times 10^{26}$ sec$^{-2})$ and the dashed curve represents the calculations of mass defects only.
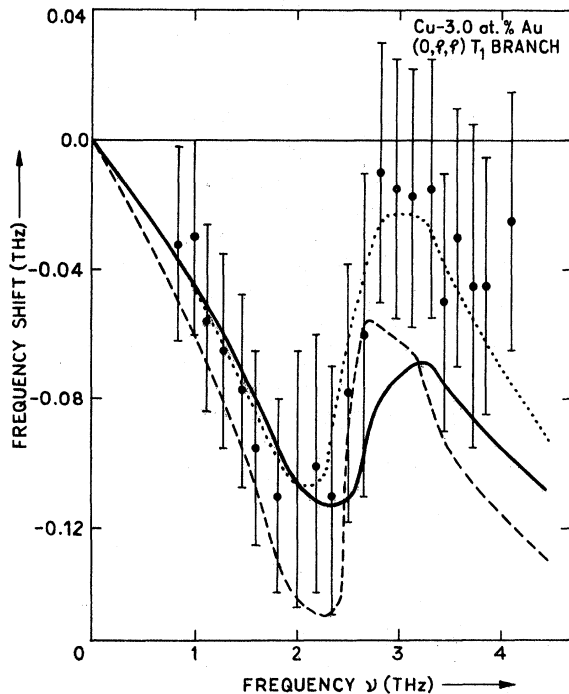
FIG. 10. Cu-3.0-at.%-Au alloy: the calculated frequency shifts in $(0, \xi, \xi)$ T_1 branch (volume effect included). The solid curve shows the present calculations with force-constant changes $(\lambda = 1.200 \times 10^{26}$ sec^{-2} and λ' $= -0.025 \times 10^{26}$ sec$^{-2})$ and the dashed curve represents the calculations of mass defects only. The solid circles represent the experimental measurements of Svensson and Kamitkahara (Ref. 3). The calculated results of Brüno and Taylor (Ref. 12) are shown by the dotted curve.

found to be unsuccessful.

The obtained phonon widths are in good agreement with those of the experimental ones in both the measured symmetry directions. In the $(0, \xi, \xi)$ T_1 branch, the calculated widths show maxima at the appropriate place but the maximum values are smaller than the experimental ones. The observed values tend to higher values in the high-frequency region. In the $(0, 0, \xi)$ symmetry direction again the place of maxima (at the resonance frequency) is approximately reproduced and the calculated values are in good agreement with the experimental ones except for some discrepancies in the low-frequency region where the calculated values are large.

C. Cu–9-at.% Au

In this alloy, one may expect to observe the high-impurity-concentration effects. However, we have shown the frequency shifts and phonon widths calculated on the basis of a low-concentration theory in Figs. 14–19. In the two transverse-polarization branches $(0, \xi, \xi)T_1$ and $(0, 0, \xi)T$, the calculated

resonant frequencies are seen to be smaller than the experimental ones. This appears to be true if we examine further the calculated phonon widths which have been compared with the experimental results in Figs. 16 and 17. The fitted curves can be definitely improved if we vary the force-constant changes to obtain a higher value for the resonant frequency. The obtained phonon widths in the high-frequency region in the $(0, \xi, \xi)T_1$ branch are much smaller than the experimental ones (Fig. 16). They may arise due to high-concentration effects where the widths are expected to increase due to enhanced interference effects. But in the $(0, 0, \xi)T$ branch (Fig. 17), the discrepancies between the calculated and experimental widths are not seen to be so large.

For this alloy, a systematic experimental study has also been made for a $(0, 0, \xi)L$ branch. In Figs. 18 and 19, we report the results of the calculations. We observe that the calculated frequency shifts are larger than the experimental ones throughout the whole frequency range. It might appear due to large-volume effects estimated in the present calculation of the mode γ's. The use of a value which is approximately 50% of the present mode-γ value can give a very good fit to the experimental data. Finally, in Fig. 19 we observe that the predicted shape of linewidths has not appeared in the experimental measurements. The low concentration theory considered here does not hold at all for such a high concentration of impurities. Also, the inclusion of force-constant changes around an impurity has allowed enhanced interference of the impurity spaces of two nearest-neighbor impurities via phonon scattering because there are 12 nearest neighbors of an impurity. Thus the failure of low-concentration theory in discussing a high-concentration alloy is not at all amazing.

V. COMPARISON WITH BRÜNO–TAYLOR RESULTS

Very recently, Brüno and Taylor[12] have discussed the phonon shifts and widths in Cu–3-at.% Au. These authors have employed a nearest-neighbor perturbation model with a central and two different noncentral force constants. Their results for shifts and widths are very similar to the present ones for a Cu–3-at.%-Au alloy except in the high-frequency region along the $(0, \xi, \xi)$ direction where these authors have found a better agreement for the phonon shifts with the experiment. In order to account for the lattice-expansion effect, they used a Morse potential for interatomic forces and calculated the force-constant changes for five neighbors. The force constants calculated on the basis of the Morse potential for the pure-copper lattice were found to be different from those obtained by Svensson et al.[16] after analyzing the experimentally determined dispersion curves. In or-
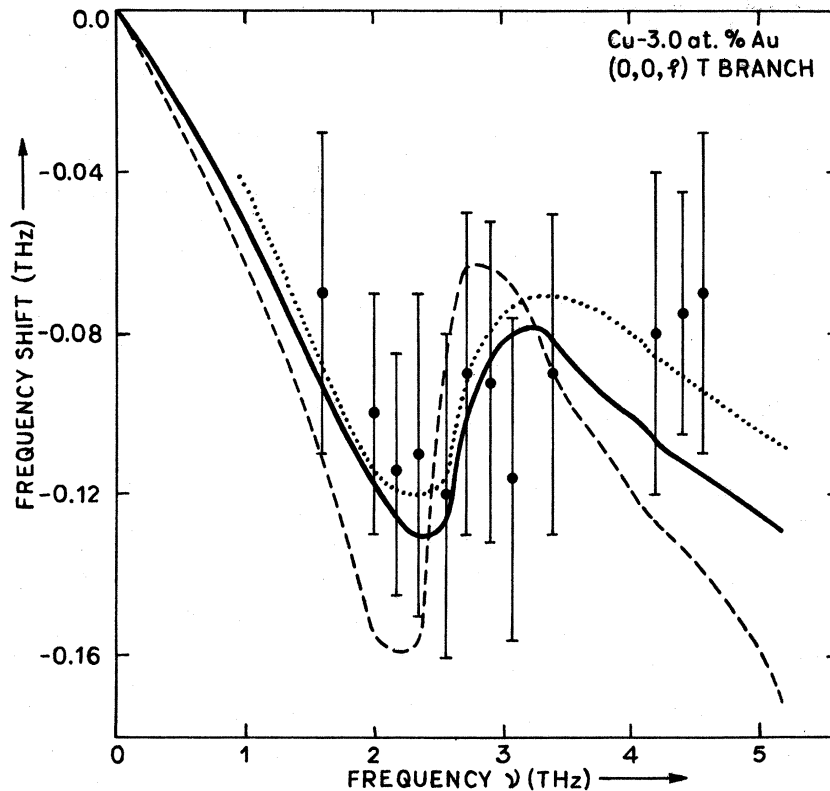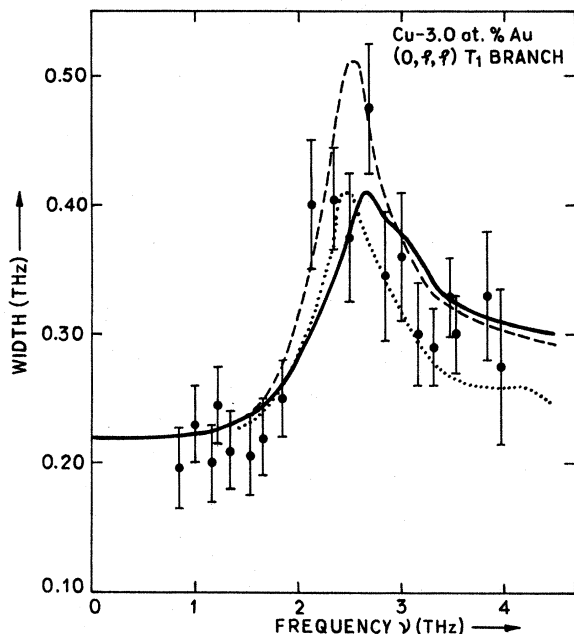
FIG. 11. Cu-3.0-at.%-Au alloy: the calculated frequency shifts in $(0, 0, \xi)$ T branch (volume effect included). The solid curve shows the present calculations with force-constant changes $(\lambda = 1.200 \times 10^{26}$ sec^{-2} and $\lambda' = -0.025 \times 10^{26}$ sec$^{-2})$ and the dashed curve represents the calculations of mass defects only. The solid circles denote the experimental measurements of Svensson and Kamitkahara (Ref. 3). The calculated results of Brüno and Taylor (Ref. 12) are shown by the dotted curve.

FIG. 12. Cu-3.0-at.%-Au alloy: the calculated phonon widths in $(0, \xi, \xi)$ T_1 branch. The solid curve shows the present calculations with force-constant changes $(\lambda = 1.200 \times 10^{26}$ sec^{-2} and $\lambda' = -0.025 \times 10^{26}$ sec$^{-2})$ and the dashed curve represents the calculations with mass defect only. The solid circles represent the experimental measurements of Svensson and Kamitkahara (Ref. 3). The calculated results of Brüno and Taylor (Ref. 12) are shown by the dotted curve.

der to obtain similar force constants, they determined percentage corrections for each of the calculated force constants. These corrections were applied to obtain the force constants for the effective lattice (i.e., the pure-copper lattice after expansion due to doping). The mode γ's were then determined after calculating the phonon frequencies for the effective lattice with these force constants. For comparison, these mode γ's are reproduced in Fig. 5. We observe appreciable structures in their mode γ's which are different from the present ones. The only advantage with their calculation was that they found a structure in the mode γ along the $(0, \xi, \xi)$ direction and the value of the mode γ was seen to be much smaller than the elastic-constant mode γ in the resonance frequency region where the experimental shifts are found to be much smaller. Consequently, their calculated negative shifts in this region were smaller in this particular branch as compared to the present ones. But there is an arbitrariness in their procedure of calculating the mode γ's. Further, the values of the elastic-constant mode γ's obtained by them for transverse branches $(0, \xi, \xi)T_1$ and $(\xi, \xi, \xi)T$ (see Fig. 5) are in disagreement with the experimental ones. Finally, a very high negative value for one of the noncentral force-constant changes obtained by them is not convincing (see Table II). On the contrary, there is no such arbitrariness in the determination of mode γ's in the present calculation and the ex-
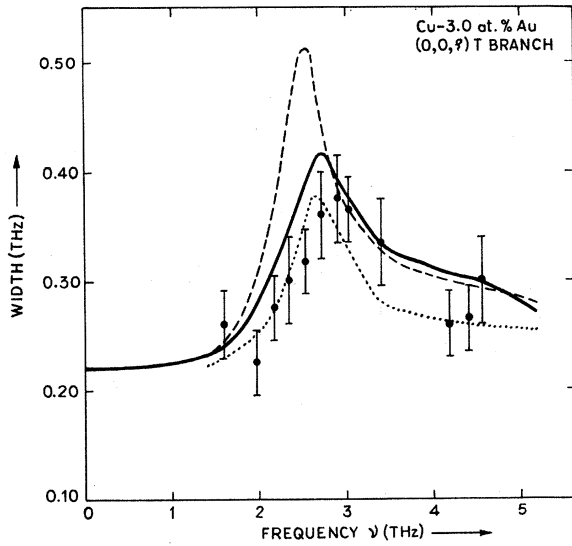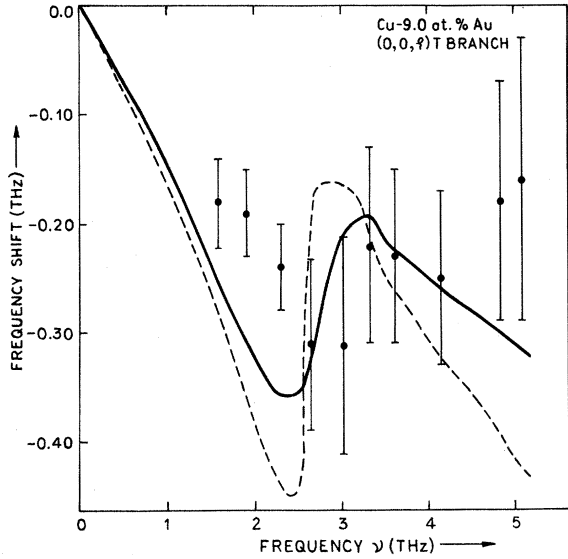
FIG. 13. Cu–3.0-at.%-Au alloy: the calculated pho-
non widths in $(0, 0, \xi)$ T branch. The solid curve shows
the present calculations with force-constant changes (λ
$= 1.200 \times 10^{26}$ sec^{-2} and $\lambda' = -0.025 \times 10^{26}$ sec^{-2}) and the
dashed curve represents the calculations of mass defects
only. The solid circles represent the experimental mea-
surements of Svensson and Kamitkahara (Ref. 3). The
calculated results of Brüno and Taylor (Ref. 12) are
shown by the dotted curve.

FIG. 15. Cu–9.0-at.%-Au alloy: the calculated fre-
quency shifts in $(0, 0, \xi)$ T branch (volume effect included).
The solid curve shows the calculations with force-constant
changes ($\lambda = 1.200 \times 10^{26}$ sec^{-2} and $\lambda' = -0.025 \times 10^{26}$ sec^{-2})
and the dashed curve represents the calculations of mass
defects only. The solid circles denote the experimental
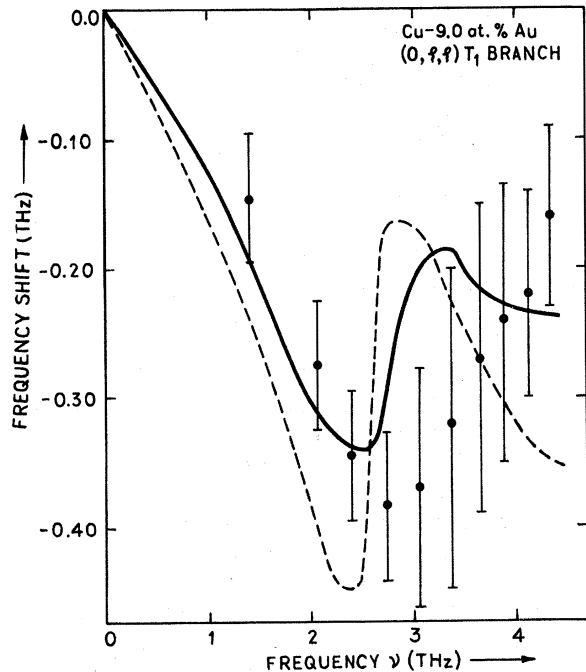measurements of Svensson and Kamitkahara (Ref. 3).

perimentally observed elastic-constant mode γ' s
are, in general, well reproduced. Also, we do
not find an inflated unphysical value for the change

FIG. 14. Cu–9.0-at.%-Au alloy: the calculated fre-
quency shifts in $(0, \xi, \xi)$ T_1 branch (volume effect in-
cluded). The solid curve shows the calculations with
force-constant changes ($\lambda = 1.200 \times 10^{26}$ sec^{-2} and λ'
$= -0.025 \times 10^{26}$ sec^{-2}) and the dashed curve represents the
calculations of mass defects only. The solid circles
represent the experimental measurements of Svensson
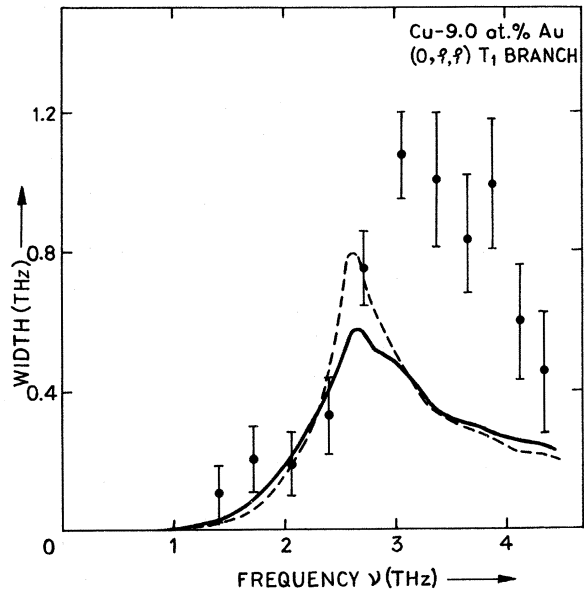and Kamitkahara (Ref. 3).

FIG. 16. Cu–9.0-at.%-Au alloy: the calculated pho-
non width in $(0, \xi, \xi)$ T_1 branch. The solid curve shows
the calculations with force-constant changes ($\lambda = 1.200$
$\times 10^{26}$ sec^{-2} and $\lambda' = -0.025 \times 10^{26}$ sec^{-2}) and the dashed
curve represents the calculations of mass defects only.
The solid circles denote the experimental measurements
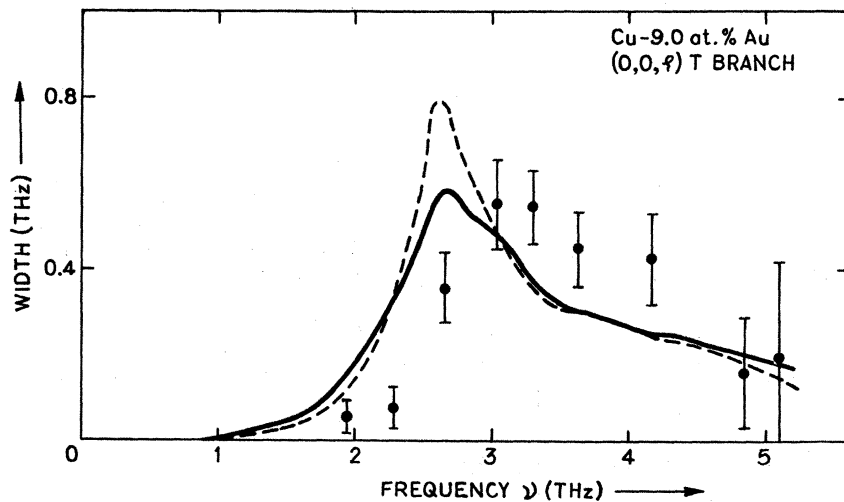of Svensson and Kamitkahara (Ref. 3).

FIG. 17. Cu-9.0-at.%-Au alloy: the calculated phonon widths in $(0, 0, \xi)$ T branch. The solid curve shows the calculations with force-constant changes ($\lambda = 1.200 \times 10^{26}$ sec^{-2} and $\lambda' = -0.025 \times 10^{26}$ sec^{-2}) and the dashed curve represents the calculations of mass defects only. The solid circles denote the experimental measurements of Svensson and Kamitkahara (Ref. 3).

in the noncentral force constant.

VI. DISCUSSION

In general, there is an over-all good agreement of the low-concentration theory with the experiment for the case of two dilute alloys containing 1- and 3-at.%-Au atoms. For a high concentration Cu−9-at.%-Au alloy, the results for the shifts and widths suggest that the experimentally measured resonant frequency is larger than that obtained in a low-concentration theory by about 15%. This increase in resonant frequency may arise due to interference between the scatterings of impurities in the crystal. This result is in agreement with that obtained earlier by Taylor[8] for isotopic impurities (see Fig.

6 of Ref. 8) in a self-consistent manner. It may be noted that the two other calculations made by Behera and Deo[17] and by Hartmann[18] have shown totally different results, i.e., the resonant frequency is seen to decrease with increase in impurity concentration. Thus, for high-concentration alloys, the Elliott–Taylor approximation does not seem to be adequate, and one should perform a self-consistent calculation such as that of Taylor.

Further, there exists discrepancies between the theory and the experiment in the high-frequency region in the $(0, \xi, \xi)T_1$ branch and in $(0, 0, \xi)L$ branch for the whole frequency range. It is not possible to remove this discrepancy by any chosen set of the parameters λ and λ'. We do not feel that
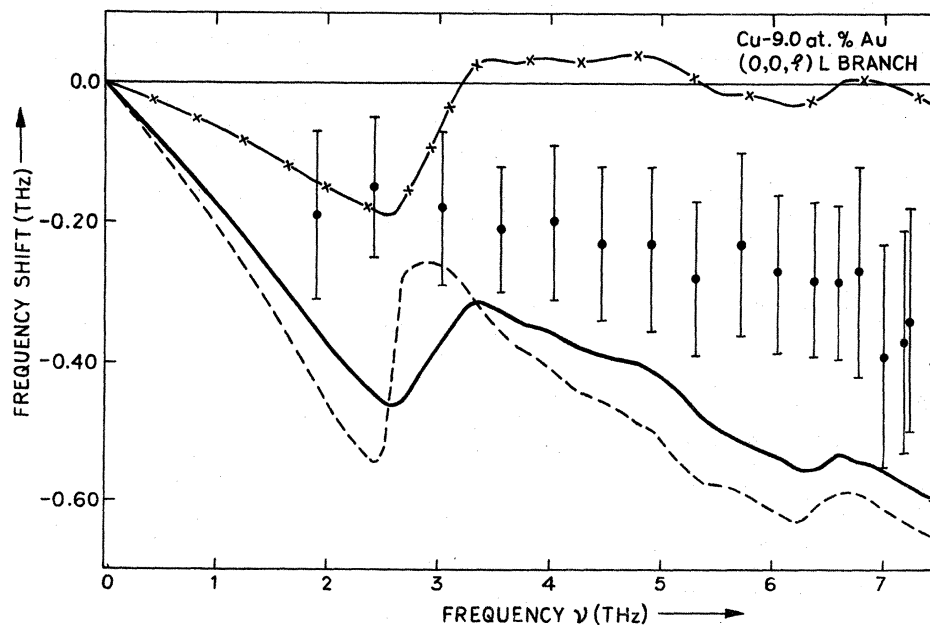

FIG. 18. Cu−9.0-at.%-Au alloy: the calculated frequency shifts in $(0, 0, \xi)$ L branch. The solid curve and the curve with crosses represents the results of force-constant changes ($\lambda = 1.200 \times 10^{26}$ sec^{-2} and $\lambda' = -0.025 \times 10^{26}$ sec^{-2}) (with and without volume effect, respectively). The dashed curve shows the calculations of mass defects only (with volume effect). The solid circles represent the experimental measurements of Svensson and Kamitkahara (Ref. 3).
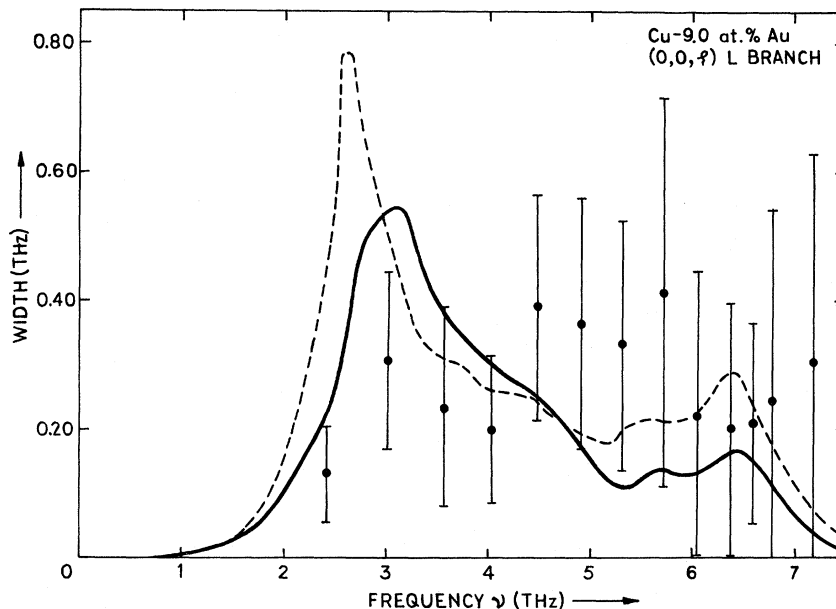
FIG. 19. Cu-9.0-at.%-Au alloy: the calculated phonon widths in $(0, 0, \xi)$ L branch. The solid curve shows the calculations with force-constant changes $(\lambda = 1.200 \times 10^{26}$ sec^{-2} and $\lambda' = -0.025 \times 10^{26}$ sec$^{-2})$ and the dashed curve shows the calculations of mass defects only. The solid circles denote the experimental measurements of Svensson and Kamitkahara (Ref. 3).

the use of a long-range perturbation associated with the impurity might be of any help in improving the results. An important source of error may arise due to incorrect calculated values of the mode γ's because the discrepancies can be removed easily if we assume smaller values for the mode γ's. Almost all the observed discrepancies between theory and experiment suggest that the mode γ's should decrease in the high-frequency region. The doping of a crystal may alter the volume-dependent effects like the screened ion-ion interaction via the electron gas. In the calculation of the mode γ's, we have not considered this effect except for a very small correction which arises in Kreb's model in a natural way due to changed interelectronic spacing in the expanded lattice. Probably, a calculation of this changed electron screening requires more attention.

VII. CONCLUSIONS

The inelastic-neutron-scattering experiments performed on dilute Cu-Au alloys can well be under-

stood on the basis of a low-concentration Green's-function theory if one includes the effects of the changed host-impurity interaction along with the effects of lattice expansion on alloying. Some observed discrepancies between theory and experiment in the high-frequency region suggest the need of the development of a more realistic theory (for the lattice-expansion effect) which properly takes into account the changes in the electron screening on alloying.

[1]E. C. Svensson, B. N. Brockhouse, and J. M. Rowe, Solid State Commun. **3**, 245 (1965).
[2]E. C. Svensson and B. N. Brockhouse, Phys. Rev. Lett. **18**, 858 (1967).
[3]E. C. Svensson and W. A. Kamitkahara, Can. J. Phys. **49**, 2291 (1971).
[4]H. B. Møller and A. R. Mackintosh, Phys. Rev. Lett. **15**, 623 (1965).
[5]A. R. Mackintosh and H. B. Møller, *Localized Excitations in Solids* (Plenum, New York, 1968), p. 721.
[6]R. M. Cunningham, L. D. Muhlestein, W. M. Shaw, and C. W. Tompson, Phys. Rev. B **2**, 4864 (1970).
[7]R. J. Elliott and A. A. Maradudin, *Inelastic Scattering of Neutrons* (International Atomic Energy Agency, Vienna, 1965),

Vol. I, p. 231.
[8]D. W. Taylor, Phys. Rev. **156**, 1017 (1967); Duscastelle, J. Phys. F **2**, 468 (1972).
[9]P. Soven, Phys. Rev. **156**, 809 (1967); Phys. Rev. **178**, 1136 (1969).
[10]K. M. Kesharwani and Bal K. Agrawal, Phys. Rev. B **6**, 2178 (1972).
[11]W. B. Daniels and C. S. Smith, Phys. Rev. **111**, 713 (1958).
[12]R. Brüno and D. W. Taylor, Can. J. Phys. **49**, 2496 (1971).
[13]R. J. Elliott and D. W. Taylor, Proc. R. Soc. Lond. **296A**, 161 (1967).
[14]Bal K. Agrawal, Phys. Rev. **186**, 712 (1969).

[15]K. Krebs, Phys. Rev. **138**, A143 (1965).

[16]E. C. Svensson, B. N. Brockhouse, and J. M. Rowe, Phys. Rev. **155**, 619 (1967).

[17]S. N. Behera and B. Deo, Phys. Rev. **153**, 728 (1967).

[18]W. Hartmann, Phys. Rev. **172**, 677 (1968).

Generalized Magnetic Pseudopotential for Noble Metals

N. C. Das and S. P. Mohanty

Department of Physics, Utkal University, Bhubaneswar-4, Orissa, India

(Received 2 November 1971)

We have obtained an expression for the magnetic pseudopotential which includes spin and spin-orbit-interaction effects and is valid for noble metals. The method consists of separating the d states in the crystal from the core states and expanding them (d states) in terms of atomic d states, core functions, and plane waves. The tight-binding functions for core and d states in the crystal and orthogonalized-plane-wave functions are constructed such that they have the symmetry of magnetic Bloch functions. These are then taken as the basis states for the wave function of the eigenstate of the problem and an effective Hamiltonian is obtained which contains the magnetic pseudopotential. This expression for the magnetic pseudopotential is further simplified and is written in a form such that it can be calculated to any order in field strength. The magnetic pseudopotentials obtained by Misra and Roth, Misra, Das, and Misra, as well as the zero-field pseudopotenial, are obtained from this expression in appropriate limits. The generalized magnetic pseudopotential can be used to calculate the total magnetic susceptibility of noble metals.

I. INTRODUCTION

Misra and Roth[1] and Misra[2] have introduced a modified pseudopotential method to treat the problem of Bloch electrons in the presence of a magnetic field. Recently Das and Misra[3] have generalized the above formulation to construct a magnetic pseudopotential which includes the effects of spin and the spin-orbit interaction. The method consists of constructing tight-binding and orthogonalized-plane-wave (OPW) functions (which have the symmetry of the magnetic Bloch functions and which form a complete set) for the wave function of the Hamiltonian of the crystal in the magnetic field. These are then used as basis states for the wave function of an eigenstate of the problem and an effective Hamiltonian is obtained which contains the magnetic pseudopotential. Thus it becomes possible to use perturbation theory to calculate different properties directly without making recourse to traditional band calculations. As an example, the diamagnetic susceptibility of simple metals[1] and metals having complicated crystal structure[4] has been calculated by this method.

However, this magnetic-pseudopotential method was not extended to noble or transition metals on the grounds of the failure of the pseudopotential approximation for these metals. The failure is, of course, due to d states which are not sufficiently localized to treat them validly as the same in the metal as in the free atom. At the same time they

retain enough of their atomic character so that if they are treated as conduction-band states, the pseudo-wave-function is not smooth, the pseudopotential is very large, and perturbation theory becomes inapplicable. This difficulty has, however, been overcome by Harrison's[5] generalization of the simple-metal pseudopotential method to the case of transition and noble metals. Harrison's pseudopotential for noble and transition metals does not contain spin or spin-orbit-interaction effects and is constructed for a field-free case.

In a recent paper Borchi and De Gennaro[6] have reformulated Harrison's[5] pseudopotential method for noble metal and have then directly generalized the Misra–Roth[1] theory to the case of noble metals. But they have not included spin and spin-orbit-interaction effects in their formulation.

In the present paper we construct a generalized magnetic pseudopotential for noble metals which will include the effects of spin and the spin-orbit interaction. Following Borchi and De Gennaro,[6] we write the d states in the metal as a linear combination of atomic d states, atomic core states, and plane waves. We also construct an OPW in which, in addition to projection to core states, projection to metallic d states is explicitly included. This is then taken as the conduction state and the Misra–Roth's[1] procedure is invoked to formulate the pseudopotential. Thus an expression for the general magnetic pseudopotential for noble metals is obtained in a form such that it can be